

**EFFECTS OF SHELL STRUCTURE IN REACTIONS  
LEADING TO THE SAME COMPOUND NUCLEUS OR  
DIFFERENT ISOTOPES \***

A.K. NASIROV<sup>†</sup>

*Bogoliubov Laboratory of Theoretical Physics, JINR, 141980 Dubna, Russia  
E-mail: nasirov@thsun1.jinr.ru*

A.I. MUMINOV

<sup>†</sup> *Institute of Nuclear Physics 702132 Ulugbek, Tashkent, Uzbekistan  
E-mail: ion@suninp.tashkent.su*

G. FAZIO, G. GIARDINA, A. LAMBERTO, R. RUGGERI, A. TACCONI

*Istituto Nazionale di Fisica Nucleare, Sezione di Catania, and  
Dipartimento di Fisica dell'Università di Messina, 98166 Messina, Italy  
E-mail: giardina@nucleo.unime.it*

F. HANAPPE

*Université Libre de Bruxelles, CP 229, B-1050 Bruxelles, Belgium  
E-mail: fhanappe@ulb.ac.be*

R. PALAMARA

*Facoltà di Architettura dell'Università di Reggio Calabria, Italy  
E-mail: rpalamara@unirc.it*

L. STUTTGE

*Institut de Recherches Subatomiques, F-67037 Strasbourg Cedex 2, France  
E-mail: stuttge@in2p3.fr*

The role of the entrance channel in fusion-fission reactions was studied by the theoretical analysis of the experimental evaporation residue excitation functions for reactions leading to the same compound nucleus. The evaporation residues cross sections for  $xn$ -channels were calculated in the frame of the combined dinuclear system concept (DNS) and advanced statistical model (ASM). The revealed differences between experimental data on the evaporation residues in the  $^{40}\text{Ar}+^{176}\text{Hf}$ ,  $^{86}\text{Kr}+^{130}\text{Xe}$  and  $^{124}\text{Sn}+^{92}\text{Zr}$  reactions leading to the  $^{216}\text{Th}^*$  compound nucleus (CN) are explained by the different spin distributions of compound nuclei which are formed. It is shown that the intrinsic fusion barrier  $B_{fus}^*$  and size of potential well are different for every entrance channel.

---

\*Talk given at the International Conference on Nuclear Physics at Border Lines, NPBL2001, Lipari (Messina, Italy), 21-24 May, 2001

## 1 Introduction

An appropriate way to understand the mechanism of the fusion-fission process in heavy ion collisions is the analysis and comparison of the measured excitation functions of evaporation residues for reactions leading to the same compound nucleus. Theoretical calculations performed in the framework of the model including the nuclear shell effect and shape of colliding nuclei allow us to come to useful conclusions about the mechanism of fusion-fission process. Often excitation functions of evaporation residues measured in various reactions leading to the same compound nucleus are different not only by the position of the maximum but also by the value of their maximums. The question on what characteristics of nuclei or what relevant degrees of freedom of the fusion-fission process are responsible for such difference in evaporation residue cross sections is a well actual problem to reveal optimal conditions for the synthesis of new super-heavy elements.

## 2 Evaporation residue production in the DNS concept

In the dinuclear system concept<sup>1</sup> the evaporation residue cross section is factorized as follows:

$$\sigma_{er}(E) = \sum_{\ell=0}^{\infty} (2\ell + 1) \sigma_{\ell}^{fus}(E, \ell) W_{sur}(E, \ell). \quad (1)$$

Here the effects connected with the entrance channel are included by the partial fusion cross section  $\sigma_{\ell}^{fus}(E)$  which is defined by the expressions:

$$\sigma_{\ell}^{fus}(E) = \sigma_{\ell}^{capture}(E) P_{CN}(E, \ell), \quad (2)$$

$$\sigma_{\ell}^{capture}(E) = \frac{\lambda^2}{4\pi} \mathcal{P}_{\ell}^{capture}(E), \quad (3)$$

where  $\lambda$  is the de Broglie wavelength of the entrance channel,  $P_{CN}(E, \ell)$  is a factor taking into account the decrease of the fusion probability due to break up of the dinuclear system before fusion;  $\mathcal{P}_{\ell}^{capture}(E)$  is the capture probability which depends on the collision dynamics and determines the amount of partial waves leading to capture.

The number of the partial waves was obtained by solving the equation of motion for the relative distance and orbital angular momentum

$$\mu(R(t)) \ddot{\mathbf{R}} + \gamma_R(R(t)) \dot{\mathbf{R}}(t) = - \frac{\partial V(R(t))}{\partial R}, \quad (4)$$

$$\frac{dL}{dt} = \gamma_{\theta}(R(t)) \left( \dot{\theta} R_{eff}^2 - \dot{\theta}_1 R_{1eff}^2 - \dot{\theta}_2 R_{2eff}^2 \right), \quad (5)$$

where  $R(t)$  is the relative motion coordinate,  $\mathbf{R}(t)$  is the corresponding velocity;  $\dot{\theta}$ ,  $\dot{\theta}_1$  and  $\dot{\theta}_2$  are angular velocities of the dinuclear system and its fragments, respectively;  $\gamma_R$  and  $\gamma_\theta$  are the friction coefficients for the relative motion along  $R$  and tangential motion when two nuclei roll on each other's surfaces, respectively;  $V(R)$  is the nucleus-nucleus potential;  $\mu(R(t))$  is the reduced mass of the system;  $R_1$  and  $R_2$  are the fragment radii.

Calculations showed that use of these kinetic coefficients leads to gradual dissipation of kinetic and rotational energy <sup>2</sup>. It was shown that at collisions of massive nuclei despite of continuous dissipation the capture becomes impossible at larger values of beam energy than the Coulomb barrier, because of the small size of the well in the nucleus-nucleus potential. The dissipation is not sufficient to trap colliding nuclei in the potential well to create a necessary condition for fusion, and in this case the formed dinuclear system undergoes quasi-fission. The nucleus-nucleus potential  $V(R)$  depends on the mutual orientations of the symmetry axes of deformed nuclei relative to  $\mathbf{R}(t)$ . The quadrupole ( $2^+$ ) and octupole ( $3^-$ ) collective excitations in spherical nuclei are taken into account. Thus, it is possible to consider fusion at different initial orientations of the symmetry axes.

The competition between fusion and quasi-fission is taken into account by the factor  $P_{CN}(E, \ell)$  which is calculated using the method developed in <sup>1</sup>, in framework of the statistical model. It was suggested that the probability of realizing the complete fusion (in competition with the quasi-fission, starting from an entrance channel that gives a DNS), is related to the ratio of level densities, depending on the intrinsic fusion or quasi-fission barriers, by the expression:

$$P_{CN} = \frac{\rho(E_{DNS}^* - B_{fus}^*)}{\rho(E_{DNS}^* - B_{fus}^*) + \rho(E_{DNS}^* - B_{qf})}, \quad (6)$$

where  $\rho(E_{DNS}^* - B_K^*)$  is the level density.

In Eq. (6),  $B_{qf}$  is the barrier of the nucleus-nucleus interaction potential which needs to be overcome if the dinuclear system decays in two fragments, and  $E_{DNS}^*$  is the excitation energy of the dinuclear system given by the difference between beam energy  $E_{c.m.}$  and the minimum of the nucleus-nucleus potential ( $E_{DNS}^* = E_{c.m.} - V(R_m)$ ).

The advanced statistical model (ASM), described in detail in <sup>3,4</sup>, allows us to take into account the dynamical aspect of the fission-evaporation competition at the compound nucleus evolution along the de-excitation cascade. Particular attention is devoted to the determination of the level densities.

Dissipation effects, which delay fission, are treated according to <sup>5,6</sup>. These include Kramers' stationary limit <sup>7</sup> and an exponential factor applied to

Kramers' fission width to account for the transient time, after which the statistical regime is reached. The systematic obtained by Bhattacharya *et al.*<sup>8</sup> gives the possibility of taking into account the incident energy per nucleon  $\epsilon$  and compound nucleus mass  $A_{cn}$  dependencies of the reduced dissipation coefficient  $\beta_{dis}$ .

According to dinuclear system concept<sup>1,9</sup>, the fusion of two colliding nuclei is possible if the following two conditions are satisfied. The first one is overcoming Coulomb barrier along axis connecting nuclear centers by nuclei at incoming stage of collision and formation of the nuclear composite system (molecular alike so called dinuclear system). This process is called a capture. The second condition is the transformation of the dinuclear system into the more compact compound nucleus overcoming the intrinsic barrier ( $B_{fus}^*$ ) which must be overcome by system during the motion on the mass (charge) asymmetry axis. So this stage is a fusion and it is realized by nucleon transfer from the light nucleus on the unoccupied states of heavy one at the limited size of overlap volume of nucleon density. For light and mediate nuclear system or for heavy nuclear system with largest mass asymmetry this  $B_{fus}^*$  barrier is very small or equal to zero and capture leads immediately to fusion. Therefore for those cases fusion cross section is calculated in frame of well known models. The barrier  $B_{fus}^*$  is determined by the difference between the maximum value of a driving potential and its value at the point corresponding to the initial charge asymmetry of the considered reaction (Fig.1). A driving potential holds significance in consideration of the fusion process as a motion of system along the charge (mass) asymmetry degree of freedom. Therefore, here more attention should be paid to that. It is obtained from the potential energy surface  $U(A, Z; R, \ell)$  as a function of masses (charges)  $A_1, A_2$  ( $A_2 = A_{tot} - A_1$ ) of fragments forming the dinuclear system at the  $R_m$  value of internuclear distance corresponding to the minimum of their nucleus-nucleus potential  $V(R)$ <sup>9</sup>. The driving potential  $U(A, Z; \ell)$  calculated in this way is presented in Fig.1. The distribution of neutrons between two fragments by the given proton numbers  $Z_1$  and  $Z_2$  (or ratios  $A_1/Z_1$  and  $A_2/Z_2$  for the both of fragments) was determined by minimizing of potential  $U(A_1, Z_1; R)$  as a function of  $A_1$  for each  $Z_1$ .

$$U(A, Z; R_m, \ell) = B_1 + B_2 + V_0(Z, \ell, \beta_1, \alpha_1; \beta_2, \alpha_2; R_m) - (B_0 + V_{CN}(\ell)), \quad (7)$$

where,  $B_1, B_2$  and  $B_0$  are the binding energies of the nuclei forming a dinuclear system and of the compound nucleus, respectively. The values of  $B_i (i = 0, 1, 2)$  were obtained from<sup>10</sup>;  $\beta_i (i = 1, 2)$  are the fragment deformation parameters and  $\alpha_i$  are the orientations of nuclei symmetry axis relative to the beam direction;  $V_{CN}(\ell)$  is the rotational energy of the compound nucleus. The

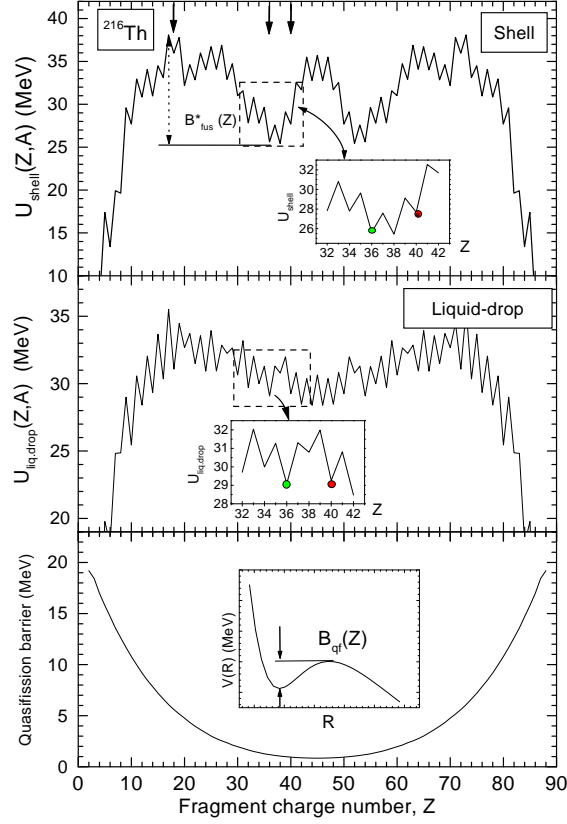


Figure 1. Driving potential  $U(Z, A, R_m; l = 0)$  as function of the charge number  $Z$  of a fragment of dinuclear system calculated by using of binding energies from the mass table<sup>9</sup> (top panel) and liquid-drop model (middle-panel). The vertical arrows indicate initial charge number of light nuclei in the  $^{40}\text{Ar} + ^{176}\text{Hf}$  (I),  $^{86}\text{Kr} + ^{130}\text{Xe}$  (II) and  $^{124}\text{Sn} + ^{92}\text{Zr}$  (III) reactions leading to  $^{216}\text{Th}$ . The intrinsic  $B_{\text{fus}}^*$  (top panel) and quasifission  $B_{\text{qf}}$  (bottom panel) barriers are shown as a function of charge number of a fragment of dinuclear system.

$R_m$  is the position of the minimum of the nucleus-nucleus potential (bottom of the pocket) on the  $R$  axis for a given mass asymmetry  $A_1$ . The smallest value of excitation energy of the compound nucleus ( $E_{CN}^{*(min)}$ ) is determined by the absolute maximum value of the driving potential laying on the way to fusion ( $Z = 0$ ) from the point corresponding to the initial charge asymmetry (Fig.1)

for the given mutual orientations of the axial symmetry axes of the projectile- and target-nucleus. Because the shapes of the potential energy surface and driving potential depend on the orientations of nuclei relatively to axis connecting the centers of interacting nuclei. The presented results on capture and fusion cross sections are obtained by averaging over contributions of different orientations. The quasi-fission is a decay of dinuclear system moving along  $R$  in the  $V(R)$  nucleus-nucleus interaction potential without reaching compact shape. Thus, for quasi-fission, it is necessary to overcome the Coulomb barrier on the  $R$  axis from internal side. The DNS concept allows one to reveal a reason of the strong decrease in the fusion cross section for a massive system or for a symmetric entrance channel due to the increase of  $B_{fus}^*$ .

### 3 Comparison of DNS model results and experimental data

#### 3.1 Reactions leading to $^{216}\text{Th}$

The role of the entrance channel on the formation of the compound nucleus and evaporation residues is a main point of our interest. The qualitative difference between fusion excitation functions of reactions leading to the same compound nucleus allows us to analyze the effect of the shell structure on the fusion mechanism. Experimental excitation functions of the evaporation residues measured in  $^{86}\text{Kr} + ^{130,136}\text{Xe}$  <sup>11</sup> reactions in the Flerov Laboratory (Dubna) and that for the  $^{40}\text{Ar} + ^{176}\text{Hf}$  <sup>12,13</sup> and  $^{124}\text{Sn} + ^{92}\text{Zr}$  <sup>14</sup> reactions have been compared with the results of calculation in the frame of the method presented in<sup>9</sup>. It is shown that the effect of shell structure is revealed in the differences at comparison of spin distributions of compound nucleus formed by using different reactions.

Experimental data reveal that the maximum value of the evaporation residue for  $^{40}\text{Ar} + ^{176}\text{Hf}$  (I) is twelve times larger than for  $^{86}\text{Kr} + ^{130}\text{Xe}$  (II) and three times larger than for  $^{124}\text{Sn} + ^{92}\text{Zr}$  (III) (see Fig.2). Because the  $^{40}\text{Ar} + ^{176}\text{Hf}$  reaction has largest charge asymmetry ( $\eta_Z = (Z_2 - Z_1)/(Z_1 + Z_2)$ ) in comparison with two others (II,III) and the height of barrier  $B_{fus}^*$  in the way to fusion for this reaction is smaller than that for (II,III) (Table 1). The way to fusion is longer for the dinuclear system which has more mass symmetric configuration. In Figs.2a and 2b, the excitation functions of the capture and fusion calculated in the frame of dinuclear system for the (I,II,III) reactions are compared. The excitation functions of the evaporation residue calculated in the frame of advanced statistical model<sup>3</sup> are in good agreement with the experimental data (see Fig.2c). At these calculations, spin distributions for CN were found by the method presented in<sup>9</sup>.

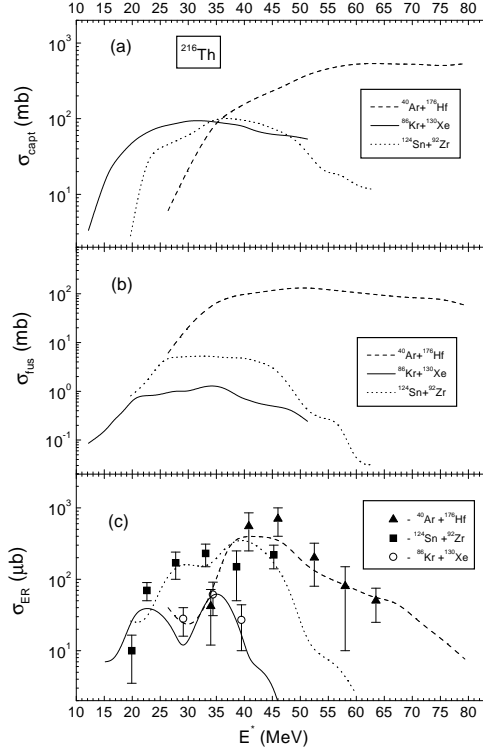


Figure 2. Comparison of the calculated capture (a) and fusion excitation function (b) as well as calculated total excitation functions of evaporation residue with the experimental data (c) for  $^{40}\text{Ar}+^{176}\text{Hf}$ <sup>12</sup>,  $^{124}\text{Sn} + ^{92}\text{Zr}$ <sup>14</sup>, and  $^{86}\text{Kr} + ^{130}\text{Xe}$ <sup>11</sup> combinations leading to the  $^{216}\text{Th}$  CN.

Table 1. Charge asymmetry, intrinsic fusion  $B_{fus}^*$ , quasi-fission  $B_{qf}$  barriers and the hindrance factor  $P_{CN}$  for the reactions leading to  $^{216}\text{Th}^*$ .

Reactions	$\eta Z$	$B_{fus}^*$ (MeV)	$B_{qf}$ (MeV)	$P_{CN}$
(I) $^{40}\text{Ar}+^{176}\text{Hf}$	0.60	2.31	7.12	0.580
(II) $^{86}\text{Kr} + ^{130}\text{Xe}$	0.20	12.31	2.35	0.014
(III) $^{124}\text{Sn} + ^{92}\text{Zr}$	0.15	9.87	1.35	0.081

But an unusual phenomenon is that the maximum value of the evaporation residue for  $^{124}\text{Sn} + ^{92}\text{Zr}$  is four times larger than for  $^{86}\text{Kr} + ^{130}\text{Xe}$  nearly at the same value of  $E_{CN}^*$ . These reactions lead to the same ( $^{216}\text{Th}^*$ ) CN. The mass asymmetry of (III)  $((A_2 - A_1)/(A_1 + A_2)=0.148)$  is smaller than one of (II) (0.203). It is not clear from the driving potential calculated using the binding energies  $B_1, B_2$  and  $B_{CN}$  determined by the liquid-drop model (see middle panel of Fig.1), since the value of the fusion barrier  $B_{fus}^*$  for the  $^{124}\text{Sn} + ^{92}\text{Zr}$  reaction is not lower than that for the  $^{86}\text{Kr} + ^{130}\text{Xe}$  reaction.

The reason of this phenomenon can be account for by comparison of driving potentials calculated using binding energies obtained from the mass table<sup>10</sup> and that determined by liquid drop model (see Fig.1, top and middle panels, respectively). The values of driving potential corresponding to the  $^{86}\text{Kr} + ^{130}\text{Xe}$  and  $^{124}\text{Sn} + ^{92}\text{Zr}$  reactions in the top and middle panel are different. One can see that, in the top panel of Fig.1, intrinsic fusion barriers for  $B_{fus}^*$  for the  $^{86}\text{Kr} + ^{130}\text{Xe}$  reaction is larger than that  $^{124}\text{Sn} + ^{92}\text{Zr}$  reaction. In this case, the hindrance factor  $P_{CN}$  of the fusion cross cross is larger for the former reaction than last one. This corresponds to the observed phenomenon for these two reactions. This discloses even qualitatively difference between values of  $B_{fus}^*$  for reactions (II) and (III). It is seen from the middle panel of Fig.1 that  $B_{fus}^*(II) \approx B_{fus}^*(III)$  when the driving potential is calculated using the binding energies  $B_1, B_2$  and  $B_{CN}$  using the liquid-drop model. If the last case takes place then a difference between the fusion excitation function of the  $^{86}\text{Kr} + ^{130}\text{Xe}$  and  $^{124}\text{Sn} + ^{92}\text{Zr}$  reactions must be very small. This is in contradiction with experimental data and that means using of binding energies obtained in the liquid-drop model is not suitable to analyze such unusual phenomenon. As seen from the Table 1 for the former reaction  $B_{fus}^*$  is larger than for the latter one due to shell effects for nuclear binding energy in the range of charge number of light fragment  $Z = 30 \div 40$ .

Another reason is seen from the analysis of spin distributions of compound nuclei formed in these three reactions.

As seen from Fig.3, spin distribution of CN formed in reaction (I) (top panel) has largest volume in comparison for the reactions (II) (middle panel) and (III) (bottom panel). It is an expected result. The matter is that why the volume of in spin distributions of CN corresponding to reaction (III) is larger than that for reaction (II). This could be connected with the  $\sigma_l^{capture}(E)$  and  $P_{CN}$  which determine partial fusion cross sections (2). The last is calculated from the equation of motion. The number of partial waves  $\ell$  which contribute to  $\sigma_l^{capture}(E)$  is determined by the size of the potential well in the entrance channel (the high of quasi-fission barrier  $B_{qf}$ ) and the friction coefficient of the radial motion. The use of the calculated friction coefficients leads to a

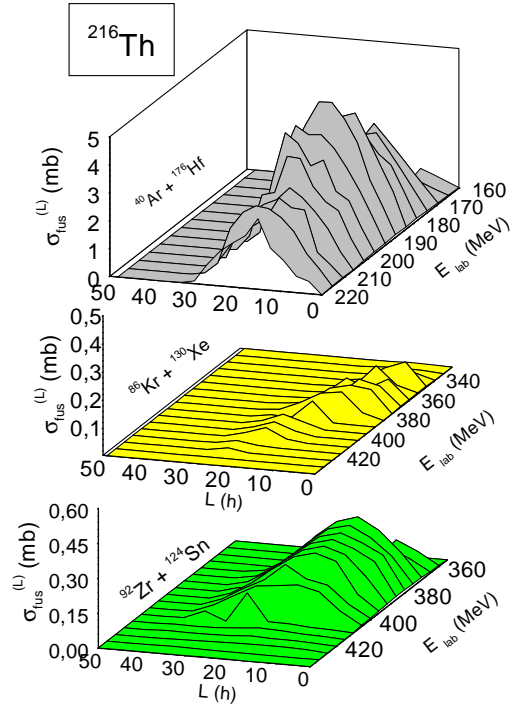


Figure 3. Spin distributions for the  $^{40}\text{Ar}+^{176}\text{Hf}$  (top panel),  $^{86}\text{Kr} + ^{130}\text{Xe}$  (middle) and  $^{124}\text{Sn} + ^{92}\text{Zr}$  (bottom) reactions.

gradual dissipation of kinetic and rotational energies<sup>2</sup>. It was shown that by collisions of massive nuclei, despite of continuous dissipation, the capture becomes impossible at beam energy values larger than the Coulomb barrier because of the small size of the well in the nucleus-nucleus potential which is a function of  $R$ . The dissipation is not enough to trap colliding nuclei in the potential well to create a necessary condition for fusion at low values of angular momentum which allow to the dinuclear system to fuse. At largest values of beam energy, capture is possible only for high angular momentum. In this case the formed dinuclear system can exist as a molecular state forming a super-deformed shape or undergoes quasi-fission because  $B_{fus}^*$  increases by angular momentum of dinuclear system. Then the maximum value of driving potential increases more faster than its value corresponding to charge (mass) asymmetry of the entrance channel. Therefore the maximum of the calculated

Table 2. Charge asymmetry, intrinsic fusion  $B_{fus}^*$ , quasi-fission  $B_{qf}$  barriers and the hindrance factor  $P_{CN}$  for the reaction leading to  $^{222}\text{Th}^*$ .

Reactions	$\eta_Z$	$B_{fus}^*$ (MeV)	$B_{qf}$ (MeV)	$P_{CN}$
(II) $^{86}\text{Kr} + ^{130}\text{Xe}$	0.20	12.31	2.35	0.014
(IV) $^{86}\text{Kr} + ^{136}\text{Xe}$	0.20	7.52	4.05	0.027

spin distributions has tendency to move to larger values of angular momentum at beam energies well above the Coulomb barrier.

This is seen in the spin distributions for the  $^{124}\text{Sn} + ^{92}\text{Zr}$  and  $^{86}\text{Kr} + ^{130}\text{Xe}$  reactions (Fig.3). The driving potential is the same for all the reactions leading to the same compound nucleus. Therefore the intrinsic fusion barriers for these reactions under discussion can be compared. It is seen in Fig.1 (top panel) from the curve of the driving potential that  $B_{fus}^*$  is smaller for the reaction (III) than for (II). This is connected with the increase of the potential energy at  $Z > 37$  due to the shell effects.

The calculation of the driving potential using binding energies determined by liquid drop model shows that in this case the shape of the curve is different than one calculated using values of binding energies from the mass table in <sup>10</sup>. Therefore, an observed smallness of the excitation function of evaporation residues for the  $^{86}\text{Kr} + ^{130}\text{Xe}$  reaction than that for  $^{124}\text{Sn} + ^{92}\text{Zr}$  is concluded to be connected with the peculiarity of the shell structure of nuclear fragments forming the dinuclear system. Due to large difference between  $Q$ -values of these three reactions leading to the  $^{216}\text{Th}^*$  CN, the centers of their excitation functions are placed at different values of the excitation energy.

### 3.2 Comparison of reactions induced by $^{86}\text{Kr}$ on the $^{130}\text{Xe}$ and $^{136}\text{Xe}$ targets

Another observed interesting phenomenon was revealed at the comparison of the experimental data on reactions induced by the  $^{86}\text{Kr}$  projectile on the  $^{130}\text{Xe}$  and  $^{136}\text{Xe}$  targets. The evaporation residue in  $^{86}\text{Kr} + ^{136}\text{Xe}$  (IV) was about 500 times larger than in  $^{86}\text{Kr} + ^{130}\text{Xe}$  (II) (Fig.4c). This result is related to the two characteristics of the fusion-fission mechanism. At first, the fusion cross section calculated using the model reviewed in <sup>9</sup> for the reaction  $^{86}\text{Kr} + ^{136}\text{Xe}$  is well larger than that for  $^{86}\text{Kr} + ^{130}\text{Xe}$  (Fig.4b). It is seen from the difference in spin distributions presented in Fig.5 for these two reactions.

This difference could be explained by the two facts: the size of the well

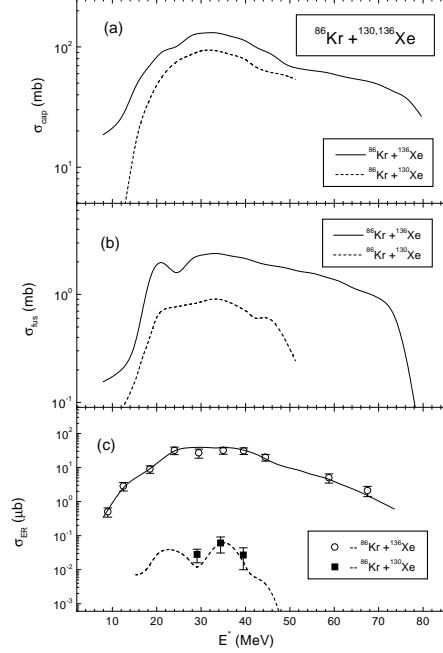


Figure 4. Comparison of the calculated capture (a), fusion (b) and evaporation residue (c) excitation functions as well as the measured excitation functions of evaporation residue (c) for the  $^{86}\text{Kr} + ^{136}\text{Xe}^{11}$  (solid curve, open circles) and  $^{86}\text{Kr} + ^{130}\text{Xe}^{11}$  (dashed curve, solid squares) reactions.

in the nucleus-nucleus potential for the  $^{86}\text{Kr} + ^{130}\text{Xe}$  (II) reaction is smaller than that for  $^{86}\text{Kr} + ^{136}\text{Xe}$  (IV) and the intrinsic fusion barrier is for the (II) reaction ( $B_{fus}^* = 12.3$  MeV) larger than for the (IV) (7.5 MeV) while the quasifission barrier  $B_{qf}$  is 2.3 MeV for the DNS obtained by  $^{86}\text{Kr} + ^{130}\text{Xe}$  and 4.05 MeV for  $^{86}\text{Kr} + ^{136}\text{Xe}$  (see Table 2).

Therefore, by comparing these two reactions, a higher value of  $B_{qf}$  (4.05 MeV against 2.3 MeV) together with a lower value of  $B_{fus}^*$  (7.5 MeV against 12.3 MeV) lead to a higher value of the fusion cross section for the reaction that gives the  $^{222}\text{Th}^*$  CN in comparison with the reaction that gives the  $^{216}\text{Th}^*$  CN. Because the excess number of neutrons in  $^{136}\text{Xe}$  makes the nuclear interaction more attractive and the potential well is more wide in comparison with the nucleus-nucleus potential between  $^{86}\text{Kr}$  and  $^{130}\text{Xe}$ . The calculated

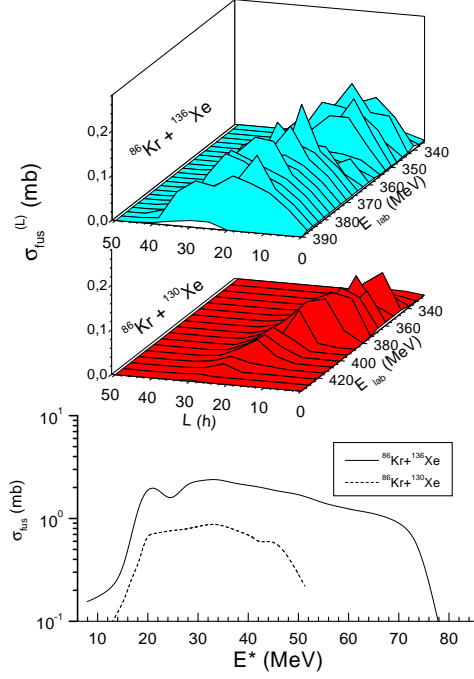


Figure 5. Spin distribution for the  $^{86}\text{Kr}+^{136}\text{Xe}$  (top panel) and  $^{86}\text{Kr} + ^{130}\text{Xe}$  (middle panel) reactions at different beam energies  $E_{lab}$ . Comparison of fusion excitation functions for these reactions (bottom panel).

excitation functions for the sum of the evaporation residues in the  $^{86}\text{Kr} + ^{130}\text{Xe}$  and  $^{86}\text{Kr} + ^{136}\text{Xe}$  reactions are shown in Fig.4c.

At second, the survival probability ( $W_{sur}$ ) of  $^{222}\text{Th}^*$  CN is larger than one of  $^{216}\text{Th}^*$ : fission barrier of the isotope  $A = 222$  is larger than for the isotope  $A = 216$  while the neutron separation energy of  $^{222}\text{Th}^*$  ( $S_n = 7.808$  MeV) is smaller than  $^{216}\text{Th}^*$  ( $S_n = 8.701$  MeV). Therefore the  $\Gamma_n/\Gamma_f$  ratio is larger for  $^{222}\text{Th}^*$  than for  $^{216}\text{Th}^*$ . For these two compound nuclei the  $\Gamma_n/\Gamma_f$  ratio is very different at each step of the two de-excitation cascades and it is larger for the cascade of  $^{222}\text{Th}^*$ . By comparing the  $\Gamma_n/\Gamma_f$  values at each step of the cascades of  $^{222}\text{Th}^*$  and  $^{216}\text{Th}^*$ , starting from the same excitation energy of the compound nuclei, in the 30-42.5 MeV excitation energy range

of CN, we find the values of the ratio  $(\Gamma_n/\Gamma_f)^{222Th^*}/(\Gamma_n/\Gamma_f)^{216Th^*}$  to be between 1.3 and 4.2 for the  $1n$ -channel; this ratio is included between 2.2 and 9.9 for the  $2n$  channel; its values are included between 3.0 and  $1.9 \times 10^5$  for the  $3n$  channel. The above-mentioned ratio is between  $2.7 \times 10^4$  and  $9.1 \times 10^5$  for the  $4n$  channel, in the 36.5-42.5 MeV excitation energy range of the compound nuclei. Large  $\Gamma_n/\Gamma_f$  values correspond to a large evaporation residue production.

#### 4 Conclusion

The combined dynamical and statistical model based on the dinuclear system approach allowed us to estimate excitation functions of quasi-fission, fusion, and formation of evaporation residues in fusion reactions with massive nuclei. The capture stage was calculated using the dynamical model and for calculation of the fusion stage a statistical approach was used. The obtained optimal beam energy or excitation energy of the compound nucleus is in good agreement with the experimental data. The fusion excitation functions calculated in this way were used to estimate the surviving probability of the formed compound nucleus relative to fission in the frame of the advanced statistical model for the de-excitation cascade. The excitation functions obtained in this paper are in good agreement with the ones measured in experiments.

The effect of the entrance channel was studied by analyzing the quantities in detail which were used in the calculation of the fusion cross section. These are the capture cross section (which is the formation probability of the dinuclear system in competition with quasi-fission), the intrinsic fusion barrier  $B_{fus}^*$ , the quasi-fission barrier  $B_{qf}$ , and the excitation energy  $E_{DNS}^*$  of the dinuclear system.

According to the scenario of the DNS-concept, the comparison of the data leading to the different  $^{216}Th^*$  and  $^{222}Th^*$  isotopes reveals a great role of the dynamics of the entrance channel and the nuclear shell structure on the mechanism of the complete fusion and the evaporation residue formation.

#### Acknowledgments

We are grateful to Prof. R.V. Jolos, Prof. V.V. Volkov, Prof. Dr. W. Scheid, Drs. G.G. Adamian, and N.V. Antonenko for helpful discussions. One of the authors (A.K.N.) thanks the INTAS (Grant No. 991-1344), the Russian Fund of Basic Research (Grant No. 01-02-16033) for financial support, and he is grateful to the STCU Uzb-45, Uzbekistan State Scientific-Technical Committee (Grant No. 7/2000) and Fund of Uzbek Academy of Science for Support of Basic Research N45-00 for partial support. A.K.N. would also like to express

his gratitude to the Università of Messina (Italy) for the warm hospitality during his stay, and to the Fondazione Bonino-Pulejo (FBP) of Messina for the help given in developing the collaboration with the group of Prof. G. Giardina.

## References

1. V.V. Volkov, N.A. Antonenko, E.A. Cherepanov, A.K. Nasirov, V.P. Permjakov, *Phys. Lett. B* **319**, 425 (1993); *Phys. Rev. C* **51**, 2635 (1995).
2. G.G. Adamian, R.V. Jolos, A.I. Muminov, A.K. Nasirov, *Phys. Rev. C* **56**, 373 (1997).
3. A. D'Arrigo, G. Giardina, M. Herman, A.V. Ignatyuk, A. Taccone, J. Phys. G **20**, 365 (1994).
4. R.N. Sagaidak, V.I. Chepigin, A.P. Kabachenko, J. Roháč, Yu.Ts. Oganessian, A.G. Popeko, A.V. Yeremin, A. D'Arrigo, G. Fazio, G. Giardina, M. Herman, R. Ruggeri, and R. Sturiale, J. Phys. G **24**, 611 (1998).
5. P. Grange and H.A. Weidenmüller, *Phys. Lett.* **96B**, (1980) 26.
6. E.M. Rastopchin, S.I. Mulgin, U.V. Ostapenko, V.V. Pashkeevich, M.I. Svirin, G.N. Smirenkin, *Sov. J. Nucl. Phys.* **53**, (1991) 741.
7. H.A. Kramers, *Physica* **7**, (1940) 284.
8. C. Bhattacharya, S. Bhattacharya, and K. Krishan, *Phys. Rev. C* **53**, (1996) 1012.
9. G. Giardina, S. Hofmann, A.I. Muminov, A.K. Nasirov, *Eur. Phys. J. A* **8**, 205 (2000).
10. G. Audi, A.H. Wapstra, *Nucl. Phys. A* **595**, 509 (1995).
11. Yu.Ts. Oganessian, A.Yu. Lavrentev, A.G. Popeko, R.N. Sagaidak, A.V. Yeremin, S. Hofmann, F.P. Heßberger, V.Ninov, Ch. Stodel, *JINR FLNR Scientific Report 1995-1996. Heavy Ion Physics*, B.I. Pustyl'nik ed., p. 62 (JINR, E7-97-206, Dubna), 1997.
12. D. Vermeulen, H.-G. Clerc, C.-C. Sahm, K.-H. Schmidt, J.G. Keller, G. Münzenberg, W. Reisdorf, *Z. Phys. A* **318**, 157 (1984).
13. H.-G. Clerc, J.G. Keller, C.-C. Sahm, K.-H. Schmidt, H. Schulte, D. Vermeulen, *Nucl. Phys. A* **419**, 571 (1984).
14. C.-C. Sahm, H.-G. Clerc, K.-H. Schmidt, W. Reisdorf, P. Armbruster, F.P. Heßberger, J.G. Keller, G. Münzenberg, D. Vermeulen, *Nucl. Phys. A* **441**, 316 (1985).